Submitted for publication in ApJ
Preprint typeset using LaTeX style emulateapj v. 01/23/15

UNCERTAINTY ON THE GALAXY-HALO CONNECTION FOR LYMAN-α EMITTERS AT $Z = 3.1$

Julián E. Mejía-Restrepo [1,3], Jaime E. Forero-Romero [2]
[1]Departamento de Astronomía, Universidad de Chile, Camino el Observatorio 1515, Santiago, Chile
[2]Departamento de Física, Universidad de los Andes, Cra. 1 No. 18A-10, Edificio Ip, Bogotá, Colombia
[3]FACom-Instituto de Física-FCEN, Universidad de Antioquia, Calle 70 No. 52-21, Medellín, Colombia
Submitted for publication in ApJ

ABSTRACT

We study the impact of cosmic variance and observational uncertainties in constraining the mass and occupation fraction ($f_{\rm occ}$) of dark matter halos hosting Lyα Emitting Galaxies at high redshift (LAEs). We use a N-body simulation to construct mock catalogs with the same typical size of observed fields at $z = 3.1$ ($\sim 1{\rm deg}^2$) to match the observed angular correlation function (ACF) and number density of LAEs. In our model a dark matter halo with mass in the range $M_{\rm min} < M_{\rm h} < M_{\rm max}$ can only host one detectable LAE at most. By following a thorough Markov Chain Monte-Carlo exploration of the parameter space determined by $M_{\rm min}$ and $M_{\rm max}$, our analysis shows that $f_{\rm occ}$ is uniquely determined by $M_{\rm min}$ regardless of $M_{\rm max}$ using the relation $f_{\rm occ} \sim 0.1 \left(M_{\rm min}/10^{10.5}\right)^{0.93}$. However, the current observational data only allows us to put weak constraints on $M_{\rm min}$, $M_{\rm max}$ and consequently on $f_{\rm occ}$. Particularly, we find that $10^{9.6}h^{-1}{\rm M}_\odot \leq M_{\rm min} \leq 10^{11.0}h^{-1}{\rm M}_\odot$, $10^{10.9}h^{-1}{\rm M}_\odot \leq M_{\rm max} \leq 10^{13.0}h^{-1}{\rm M}_\odot$ and $0.02 \leq f_{\rm occ} \leq 0.30$. Nevertheless, we also find that the upcoming large surveys can help to put tighter constraints on $M_{\rm min}$ and $f_{\rm occ}$ through the width measurement of the LAE number distribution function obtained over several fields of the same size of current observations. Analogously, the improvement in the precision of the measured ACF will assist in constraining $M_{\rm max}$.

Subject headings: Cosmology: theory - large-scale structure of Universe - Methods: data analysis - numerical - N-body simulations

1. INTRODUCTION

(●REFS)ADD NEWER REFERENCES Lyman-α emitting galaxies (LAEs) are central to a wide range of subjects in extragalactic astronomy. LAEs can be used as probes of reionization (Dijkstra et al. 2011), tracers of large scale structure (Koehler et al. 2007), signposts for low metallicity stellar populations, markers of the galaxy formation process at high redshift (Dayal et al. 2009; Forero-Romero et al. 2012) and tracers of active star formation (Guaita et al. 2013).

In most of those cases, capitalizing the observations requires understanding how LAEs are formed within an explicit cosmological context. Under the current structure formation paradigm the dominant matter content of the Universe is dark matter (DM). Each galaxy is thought to be hosted by a larger dark matter structure known as a halo. (Peebles 1980; Springel et al. 2005). Understanding the cosmological context of LAEs thus implies studying the galaxy-halo connection. Galaxy formation models suggest that the physical processes that regulate the star formation cycle are dependent on halo mass (Behroozi et al. 2013). The mass becomes the most important element in the halo-galaxy connection.

The goal becomes finding the typical DM halo mass of halos hosting LAEs. In the case of LAEs there are different ways to find this mass range. One approach is theoretical, using general astrophysical principles to find the relationship between halo mass, intrinsic Lyα luminosities and observed Lyα luminosities. This approach is usually implemented through semi-analytic models (Garel et al. 2012; Orsi et al. 2012) and full N-body hydrodynamical simulations (Laursen & Sommer-Larsen 2007; Dayal et al. 2009; Forero-Romero et al. 2011; Yajima et al. 2012).

The downside of these calculations is the uncertainty in the estimation of the escape fraction of Lyα photons. Given the resonant nature of the Lyα line, the escape fraction is sensitive to the dust contents, density, temperature, topology and kinematics of the neutral Hydrogen in the interstellar medium (ISM). The process of finding a consensus on the expected value for the Lyα escape fraction in high redshift galaxies is still matter of open debate (Neufeld 1991; Verhamme et al. 2006; Forero-Romero et al. 2011; Dijkstra & Kramer 2012; Laursen et al. 2013; Orsi et al. 2012).

A different approach to infer the typical mass of halos hosting LAEs is based on the spatial clustering information. This approach uses the fact that in CDM cosmologies the spatial clustering of galaxies on large scales is entirely dictated by the halo distribution (Colberg et al. 2000), which in turn has a strong dependence on halo mass. Using measurements of the angular correlation function of LAEs, observers have put constraints on the typical mass and occupation fraction of the putative halos hosting these galaxies (Hayashino et al. 2004; Gawiser et al. 2007b; Nilsson et al. 2007; Ouchi et al. 2010; Bielby et al. 2016). In these studies the observations are done on fields of ~ 1 deg^2 and the conclusions derived on the halo host mass do not elaborate on the uncertainty resulting from the cosmic variance on these fields.

In this letter we investigate the impact of cosmic variance in constraining the mass and occupation fraction of halos hosting LAEs at $z = 3$. We build mock surveys from a cosmological N-body to compare them against the observations in Bielby et al. (2016) using the angular correlation function. We use a simple model to populate a

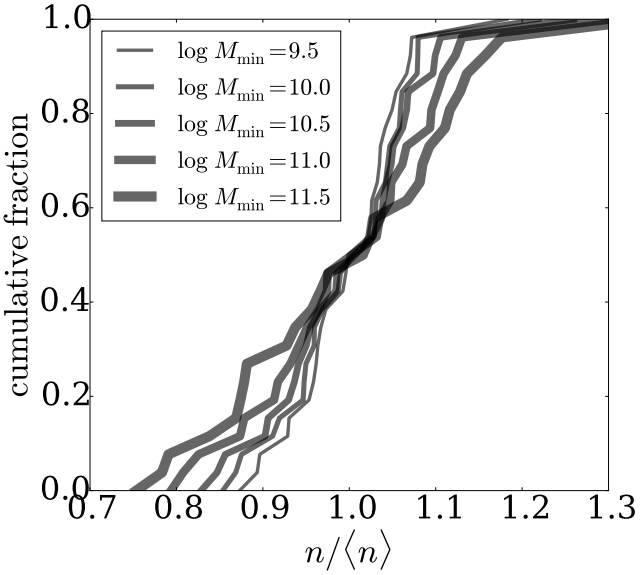

FIG. 1.— Cumulative halo number density distribution function over 27 mock fields. Each line corresponds to a different model with increasig values of $M_{\rm min}$. Different models produce different number density distributions. The width increases with $M_{\rm min}$.

halo in the simulation with a LAE assuming a minimum ($M_{\rm min}$) and maximum mass ($M_{\rm max}$) for the dark matter halos hosting LAEs without predicting a Lyα luminosity. This approach bypasses all the physical uncertainties associated to star formation and radiative transfer. We use the Markov Chain Monte Carlo technique to obtain the likelihood of the parameters given the observational constraints.

Throughout this letter we assume a ΛCDM cosmology with the following values for the cosmological parameters, $\Omega_m = 0.30711$, $\Omega_\Lambda = 0.69289$ and $h = 0.70$, corresponding to the matter density, vacuum density and the Hubble constant in units of 100 km s^{-1} Mpc^{-1}.

2. METHODOLOGY

The base of our method is the comparison between observations and mock catalogs. This approach allows us to take explicitly into account cosmic variance. The comparison has four key elements. First, the observations we take as a benchmark. Second, the N-body simulation and the halo catalogs we use to build the mocks. Third, the parameters describing our model to assign a LAE to a halo. Fourth, the statistical method we adopt to compare observations and simulations. We describe in detail these four elements in the following subsections.

2.1. *Observational constraints*

Bielby et al. (2016) used narrow band imaging to detect 643 LAE candidates at $z \sim 3$ with equivalent widths of $\gtrsim$65Å and a flux limit of 2×10^{17}erg/cm^2/s ($L \sim 7 \times 10^{42}$erg/s). Using spectroscopy they found a 22% contamination fraction. Their observations cover 5 (out of 9) independent and co-spatial fields of the VLT LBG Redshift Survey (VLRS). The total observed area corresponds to 1.07deg^2 that translates to $\sim 80^2 h^{-1}$Mpc^2 in a comoving scale. Bielby et al. (2016) used the NB497 narrow-band filter whose 77Å FWHM and 154Å FWTM correspond to a total observational depth of $44h^{-1}$Mpc and $82h^{-1}$Mpc comoving, respectively.

2.2. *Simulation and halo catalog*

We use results from the Bolshoi simulation (Klypin et al. 2011, 2014) which was performed in a cubic volume of 250 h^{-1} Mpc comoving on a side. The dark matter distribution was sampled using 2048^3 particles. The cosmological parameters are consistent with Planck results (Planck Collaboration et al. 2014) with a matter density $\Omega_{\rm m} = 0.307$, cosmological constant $\Omega_\Lambda = 0.693$, dimensionless Hubble constant $h = 0.678$, slope of the power spectrum $n = 0.96$ and normalization of the power spectrum $\sigma_8 = 0.823$. This translates into a particle mass of $m_{\rm p} = 1.5 \times 10^8\ h^{-1}\ {\rm M}_\odot$.

We use halo catalogs constructed with a Bound-Density-Maxima (BDM) algorithm. The catalogs were obtained from the publicly available Multidark database [1] (Riebe et al. 2013). For each halo in the box we extract its comoving position and mass. We focus our work on halos more massive than $1.5 \times 10^9 h^{-1}{\rm M}_\odot$ resolved with at least 10 particles. We do not take into account subhalos.

We split the simulation volume at z∼3 into 27 smaller mock volumes mimicking the area and depth reported in Bielby et al. (2016) and described in §2.1.

2.3. *A simple LAE model*

We build the simplest possible model to assign a LAE to each DM halo without trying to compute a LAE luminosity.

We first assume that a dark matter halo can host one detectable LAE at most. This assumption is consistent with theoretical analysis of the correlation function (Jose et al. 2013) and observations that confirm a lack of class pairs in LAEs Bond et al. (2009). Then we say that a halo will host a LAE with probability $f_{\rm occ}$ if and only if the halo mass is in the range $M_{\rm min} < M_{\rm h} < M_{\rm max}$. We also use the variable $\Delta M$to represent the mass range width, $\Delta M \equiv \log M_{\rm max} - \log M_{\rm max}$.

The parameter $f_{\rm occ}$ can be thought as the LAE occupation fraction of dark matter halos. An astrophysical interpretation of $f_{\rm occ}$ convolves at least three phenomena: the actual presence of a star forming galaxy in a halo, the escape fraction of Lyα radiation and its detectability as a LAE. We do not try to disentangle these complex phenomena. We instead opt for an arithmetic interpretation by setting $f_{\rm occ}$ as the ratio between the observed number of LAEs and the number of halos within the considered mass range, that is $f_{\rm occ} \equiv N_{\rm LAEs}/N_{\rm halos}$.

For each mock catalog we also randomly remove 22% LAEs to mimic the effect of contamination in observations Bielby et al. (2016). On top of that we apply rejection sampling to our LAE selection taking the transmission function of the NB479 filter used in their observations as a radial selection factor.

Fig. 1 shows the cumulative halo number density for all 27 subvolumes in the simulation, with a normalization by the average number density among fields. Each line represents a different model $\mathcal{M}$ with fixed $f_{\rm occ} = 1$ and $\Delta M = 1.0$; and varying $M_{\rm min}$, This Figure shows that the halo number density varies across sub-volumes, as an expression of cosmic variance. As a consequence, the $f_{\rm occ}$ also varies across the mock fields by the same factor

[1] http://www.multidark.org/MultiDark/

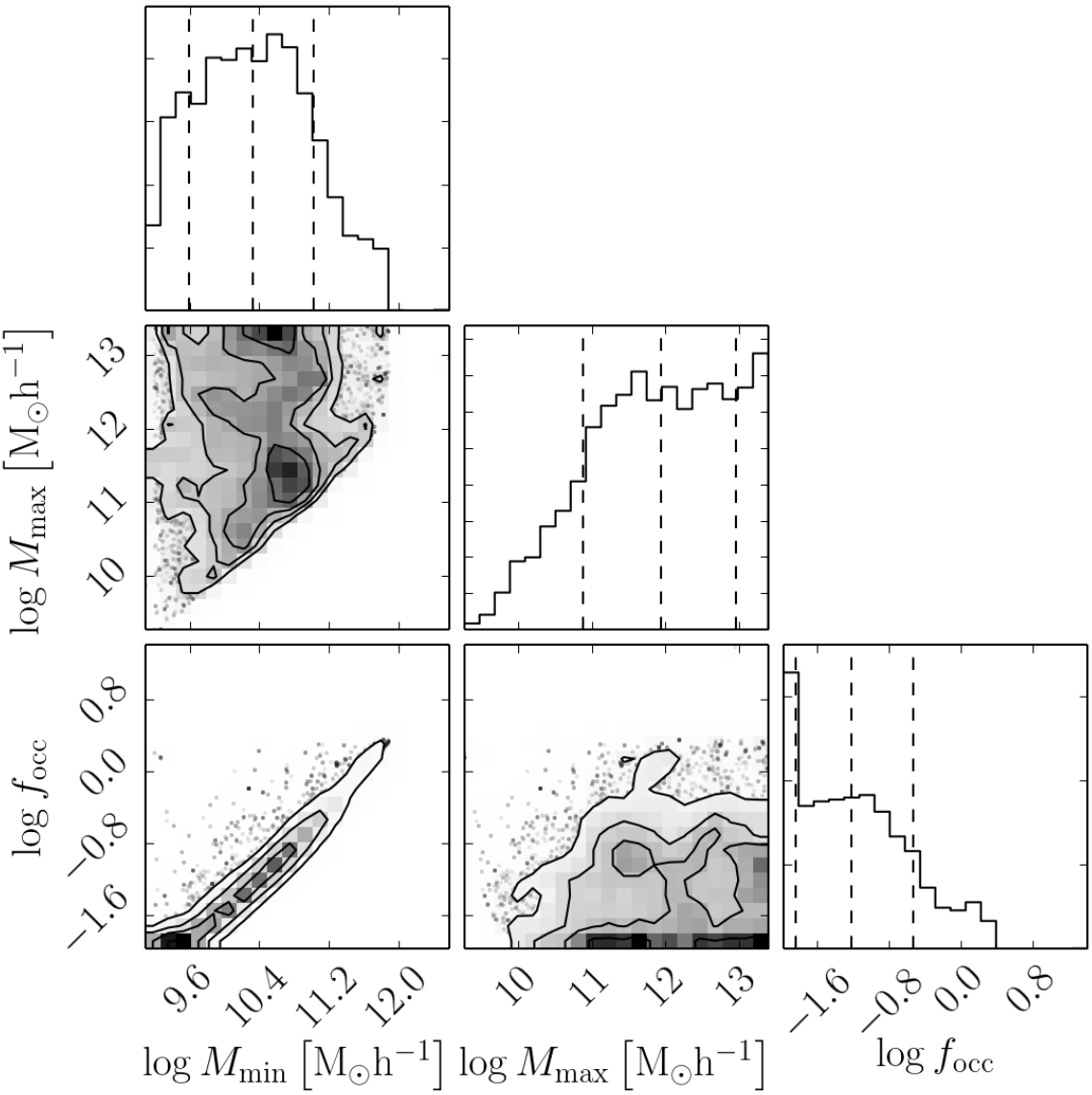

FIG. 2.— One and two dimensional projections of the posterior probability distributions of $M_{\rm min}$, $M_{\rm max}$ and $f_{\rm occ}$. The models with $\log f_{\rm occ} > 0.00$ ($f_{\rm occ} > 1$) correspond to models where the number density of halos is smaller than the number of observed LAEs but we consider them as consistent because of the uncertainty in the median number density due to cosmic variance. See Fig. 1 and §2.4 for details.

factor.

In what follows we note by the letter $\mathcal{M}$ a model defined by a particular choice of the two parameters $M_{\rm min}$, $M_{\rm max}$. For each model $\mathcal{M}$ we define $\tilde{f}_{\rm occ}$ as the median occupation fraction within the the mock fields.

2.4. *Model Selection*

We make a thorough parameter space exploration of the models $\mathcal{M}$ by means of a Markov Chain Monte Carlo technique using the EMCEE python package (Foreman-Mackey et al. 2013).

We put a flat prior on $\log M_{\rm min}$ and $\log M_{\rm max}$ between 9.2 up to 13.4, corresponding to the halo mass range of the simulation at $z = 3$. We restrict the selection to models that give a minimal number density $N_{\rm halos} > N_{\rm LAE}/3$. This means that it is possible to have $N_{\rm halos} < N_{\rm LAE}$ and hence $f_{\rm occ} \equiv N_{\rm LAE}/N_{\rm halos} > 1$. This only reflects the uncertainty in the number density of LAEs due to cosmic variance.

The MCMC exploration is done using a total of 24 seeds and 400 iterations (9600 models) to sample the posterior PDF, $P(\mathcal{M}|\text{observations}) \propto \exp(-\chi^2_{\mathcal{M}}/2)$, with the $\chi^2_{\mathcal{M}}$ based on the Angular Correlation Function (ACF),

$$\chi^2_{\mathcal{M}} = \sum_\theta \left[\frac{\left(\mathrm{ACF}_{\mathcal{M}}(\theta) - \mathrm{ACF}_{\rm obs}(\theta)\right)^2}{\sigma^2_{\mathcal{M}}(\theta) + \sigma^2_{\rm obs}(\theta)} \right] \qquad (1)$$

where $\mathrm{ACF}_{\mathcal{M}}$ and $\mathrm{ACF}_{\rm obs}$ are the ACF of the explored model $\mathcal{M}$ and the observational ACF reported by Bielby et al. (2016) respectively. $\sigma_{\mathcal{M}}$ is the associated 1-σ scatter of the $\mathrm{ACF}_{\mathcal{M}}$ as a product of cosmic variance and $\sigma_{\rm obs}$ is the observational error associated to $\mathrm{ACF}_{\rm obs}$. We compute the $\mathrm{ACF}_{\mathcal{M}}$ using the Landy & Szalay estimator

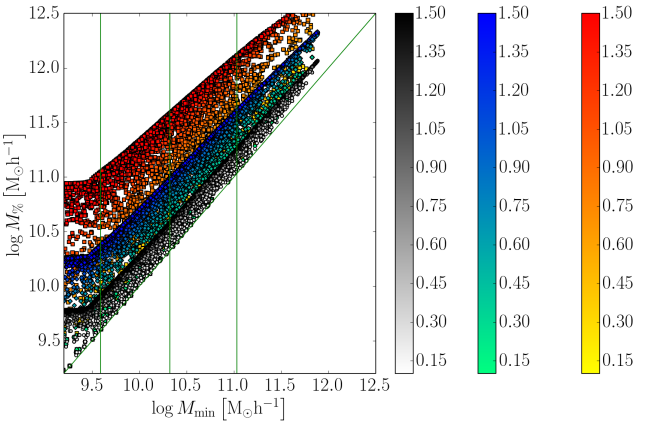

FIG. 3.— $\log M_{\rm min}$ vs $\log M_{50\%}$ (black), $\log M_{16\%}$-$\log M_{84\%}$ (blue) and $\log M_{2.5\%}$-$\log M_{97.5\%}$(red) for different values of $\log M_{\rm max}$. The points are color coded by $\Delta \log M$ [$\log M_\odot h^{-1}$]. The green line diagonal line accounts for the 1:1 relation and the green vertical lines represent the 16, 50 and 84 percentiles of the posterior probability distribution of $M_{\rm min}$.

(Landy & Szalay 1993).

3. RESULTS AND DISCUSSION

3.1. *Constraints on Model Parameters*

Fig. 2 shows the one and two dimensional projections of the posterior probability distributions of the parameters in our LAE model. This Figure represents our main result: $M_{\rm min}$, $M_{\rm max}$ and $f_{\rm occ}$ cannot be tightly constrained from the available observations.

The preferred $1-\sigma$ range for the masses is $9.6 < \log M_{\rm min} < 11.0$ and $10.9 < \log M_{\rm max} < 13.0$. $f_{\rm occ}$ is completely determined by $M_{\rm min}$ from $f_{\rm occ}$=0.015 when $\log M_{\rm min} = 9.6$ to $f_{\rm occ} = 0.30$ when $\log M_{\rm min} = 11.0$. We compute the power-law dependece between $f_{\rm occ}$ and $M_{\rm min}$ to be

$$f_{\rm occ} = 0.1 \left(\frac{M_{\rm min}}{10^{10.5} h^{-1} {\rm M}_\odot} \right)^{0.93}. \quad (2)$$

We remind to the reader that models whith $\log f_{\rm occ} > 0.00$ ($f_{\rm occ} > 1$) correspond to cases where the halo number density is smaller than the number of observed LAEs but are still consistent because of the uncertainty in the median number density of LAEs in the universe due to cosmic variance (see Fig. 1 and §2.4).

3.2. *Median Halo Mass Within Models*

We now compute the median mass, $\log M_{50}$, of the LAE hosting halos for each model $\mathcal{M}$; $\log M_{50}$ allows a direct comparison between our results and previous results in the literature (e.g. Hayashino et al. 2004; Gawiser et al. 2007a; Ouchi et al. 2010; Bielby et al. 2016) that used a more simplified approach.

In Fig. 3 we show the 50 ($\log M_{50}$, black dots), the 84 ($\log M_{84}$,blue diamonds) and 95 ($\log M_{95}$, red squares) percentiles of the LAE halo mass as a function of $\log M_{\rm min}$ for each of the models that we run in our MCMC simulation. The points are color coded according to their $\Delta \log M$ associated value. We can see that the median mass (M_{50}) and M_{84} are not very sensitive to $\log M_{\rm max} = \log M_{\rm min} + \Delta \log M$ specially when $\Delta \log M \gtrsim 1.0$dex. We particularly found that $\log M_{\rm min} \lesssim \log M_{50} \lesssim \log M_{\rm min} + 0.2$dex and that

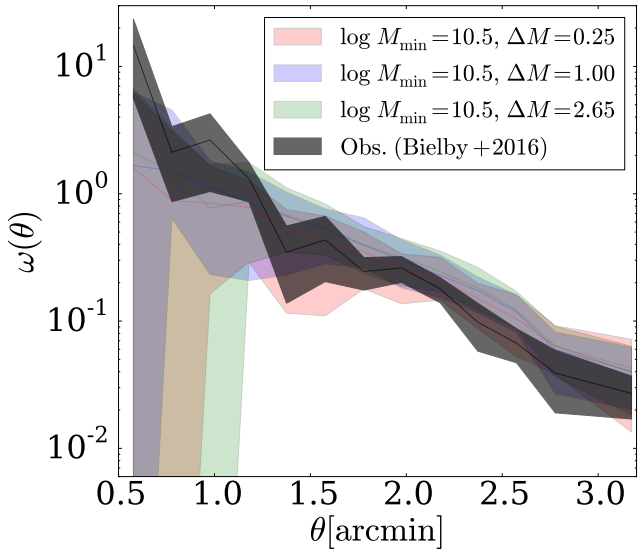

FIG. 4.— Angular Correlation functions for $\log M_{\rm min}[{\rm M}_\odot {\rm h}^{-1}] = 10.5$ and different values of ΔM. The shaded region represents the 1-sigma deviation due to cosmic variance. Radical different models in ΔM are consistent with observations once cosmic variance is modelled in detail.

$\log M_{\rm min} + 0.1$dex $\lesssim \log {\rm M}_{50} \lesssim \log {\rm M}_{\rm min} + 0.5$dex regardless of the value of $\Delta \log M$. The latter is a consequence of the very steepen distribution of the dark matter mass function and is at the same time the reason for the almost perfect one to one relation between $M_{\rm min}$ and $f_{\rm occ}$. However, it can also be seen in Fig. 3 that $\log M_{84}$ is very sensitive to $\log M_{\rm max}$($\log M_{\rm min}+0.2$dex $\lesssim \log {\rm M}_{50} \lesssim \log {\rm M}_{\rm min} + 1.5$dex). Thereby, any differences in the clustering strength of models sharing the same $M_{\rm min}$but different $M_{\rm max}$should be mainly driven by the $\sim 16\%$ most massive halos of each model $\mathcal{M}$.

In order to estimate the effect of most massive halos in $ACF_{\mathcal{M}}$ in Fig. 4 we show the computed $ACF_{\mathcal{M}}$ of models with $\log M_{\rm min} = 0.5$ and different values of $\Delta \log M$. We can see that the clustering gets stronger for larger values of $\Delta \log M$. Nevertheless, due to the large impact of cosmic variance at the volume of the current observations all the models are basically consistent within errors. The last result together with the large Poissonian observational error in the ACF explain the current difficulty to put tighter constrains in $\log M_{\rm max}$ in our model.

In Fig. 3 the green vertical lines represent the 16, 50 and 84 percentiles of the posterior probability distribution of $M_{\rm min}$that we previously obtained. From this figure we find that the median dark matter halo mass is $\tilde{M}_{\rm h} = 10^{10.6^{+0.7}_{-0.6}}$. This result is consistent with previous estimations of the median dark matter halo mass reported by Bielby et al. (2016) ($\tilde{M}_{\rm h} = 10^{11.0\pm0.6}$), Gawiser et al. (2007b) ($\tilde{M}_{\rm h} = 10^{10.9\pm0.9}$) and Ouchi et al. (2010) ($\tilde{M}_{\rm h} = 6.7^{+42.0}_{6.7} \times 10^{10}$) using semi-analitical approaches.

3.3. *Constraining Dark matter halos mass with cosmic variance*

Fig. 1 shows the halo number distribution (HND) in the mock fields of the simulation for different models $\mathcal{M}$. By simple inspection one can infer an increase in the distribution with as $\log M_{\rm min}$increase. This trend is confirmed in Fig. 5 where we plot the central 1-σ (blue diamonds) and 2-σ (red dots) widths of the NDH as a

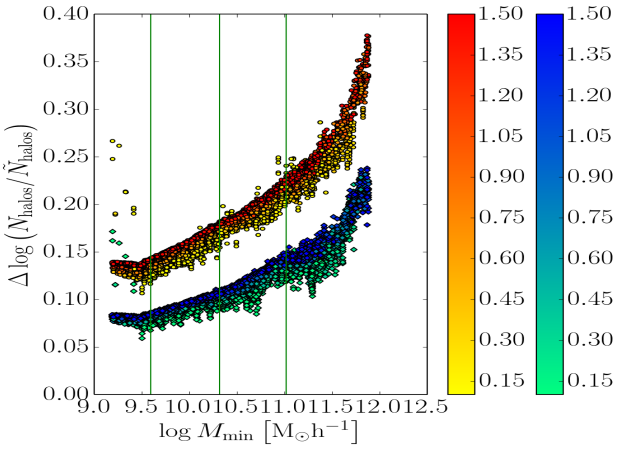

FIG. 5.— Width of the halo number distribution over the 54 mock field of the simulation ($\Delta \log\left(N_{halos}/\tilde{N}_{halos}\right)$) of the central 68 (blue diamonds) and 95(red circles) percentiles vs $M_{\rm min}$. Points are color coded according to their associated value of $\Delta M \equiv M_{\rm min} - M_{\rm min}$. The green line diagonal line accounts for the 1:1 relation and the green vertical lines represent the 16, 50 and 84 percentiles of the posterior probability distribution of $M_{\rm min}$.

function of $\log M_{\rm min}$. We particularly found that when we consider survey fields of $\sim 1{\rm deg}^2$, the central 1-σ (2-σ) width of the HND increases monotonically from 0.05dex (0.10dex) when $\log M_{\rm min} = 9.5$ to 0.20dex (0.35dex) when $\log M_{\rm min} = 12.0$. The latter result opens the possibility to constrain the $\log M_{\rm min}$(as well as the median mass) of LAEs by simply measure the width of the distribution of observed LAE along several observational fields mapping $\sim 1{\rm deg}^2$ in area and the observational depth determined by the NB479 filter.

4. CONCLUSIONS

In this letter we studied the impact of cosmic variance and observational uncertainties in constraining the mass range and occupation fraction of dark matter halos hosting LAEs. To this end, we used the BolshoiP N-body simulation to construct 27 mock fields with the same typical size of observed fields at $z = 3.1$ ($\sim 1{\rm deg}^2$). In our model a dark matter halo with mass in the range $M_{\rm min} < M_{\rm h} < M_{\rm max}$ can only host one detectable LAE at most. We explored the parameter space determined by $M_{\rm min}$ and $M_{\rm max}$ using Monte Carlo Markov-Chain minimization to match the observed ACF and mean number density of LAEs.

Our analysis allowed us to put weak constraints on $M_{\rm min}$, $M_{\rm max}$ and $f_{\rm occ}$ where $10^{9.7}h^{-1}{\rm M}_\odot \leq \log M_{\rm min} \leq 10^{11.2}h^{-1}{\rm M}_\odot$, $10^{10.9}h^{-1}{\rm M}_\odot \leq \log M_{\rm max} \leq 10^{13.0}h^{-1}{\rm M}_\odot$ and $0.02h^{-1}{\rm M}_\odot \leq f_{\rm occ} \leq 0.5$, spanning three orders of magnitude in halo mass. Previous works(Hayashino et al. 2004; Gawiser et al. 2007b; Ouchi et al. 2008; Bielby et al. 2016) have found typical masses within somehow narrower mass ranges ($\sim 10^{10.5}$-10^{12}). The main reason for our weaker constraints and large discrepancies with previous works resides in the cosmic variance on the typical field size in observations. A thorough exploration of cosmic variance impact as we present in this letter had not been presented so far in the literature.

Our analysis also allowed us to draw three results that can be used to put tighter constraints on $M_{\rm min}$, $M_{\rm max}$ and $f_{\rm occ}$ once upcoming large LAE surveys, as the HETDEX project (Adams et al. 2011) and the HSC ultra deep survey, are available :

1. $f_{\rm occ}$ and the median mass of LAEs are almost uniquely determined by $M_{\rm min}$ regardless of $M_{\rm max}$.

2. measuring the width of the LAE number distribution function obtained over several fields of ≈ 1 deg^2 one will be able to tightly constrain $M_{\rm min}$, $M_{\rm med}$ and $f_{\rm occ}$ up to a factor of 2.

3. $M_{\rm max}$ drives the ACF strength at short angular distances (< 1 arcmin), therefore precise measurements of the ACF at such scales are crucial to accurately determine $M_{\rm max}$.

ACKNOWLEDGMENTS

JM acknowledges "CONICYT-PCHA/doctorado Nacional para extranjeros/2013-63130316" for their PhD scholarship support.

The authors gratefully acknowledge the Gauss Centre for Supercomputing e.V. (www.gauss-centre.eu) and the Partnership for Advanced Supercomputing in Europe (PRACE, www.prace-ri.eu) for funding the MultiDark simulation project by providing computing time on the GCS Supercomputer SuperMUC at Leibniz Supercomputing Centre (LRZ, www.lrz.de). The Bolshoi simulations have been performed within the Bolshoi project of the University of California High-Performance AstroComputing Center (UC-HiPACC) and were run at the NASA Ames Research Center.

REFERENCES

Adams, J. J., Blanc, G. A., Hill, G. J., Gebhardt, K., Drory, N., Hao, L., Bender, R., Byun, J., Ciardullo, R., Cornell, M. E., Finkelstein, S. L., Fry, A., Gawiser, E., Gronwall, C., Hopp, U., Jeong, D., Kelz, A., Kelzenberg, R., Komatsu, E., MacQueen, P. J., Murphy, J., Odoms, P. S., Roth, M., Schneider, D. P., Tufts, J. R., & Wilkinson, C. P. 2011, ApJS, 192, 5

Behroozi, P. S., Wechsler, R. H., & Conroy, C. 2013, ApJ, 770, 57

Bielby, R. M., Tummuangpak, P., Shanks, T., Francke, H., Crighton, N. H. M., Bañados, E., González-López, J., Infante, L., & Orsi, A. 2016, MNRAS, 456, 4061

Bond, N. A., Gawiser, E., Gronwall, C., Ciardullo, R., Altmann, M., & Schawinski, K. 2009, ApJ, 705, 639

Colberg, J. M., White, S. D. M., Yoshida, N., MacFarland, T. J., Jenkins, A., Frenk, C. S., Pearce, F. R., Evrard, A. E., Couchman, H. M. P., Efstathiou, G., Peacock, J. A., Thomas, P. A., & Virgo Consortium. 2000, MNRAS, 319, 209

Dayal, P., Ferrara, A., Saro, A., Salvaterra, R., Borgani, S., & Tornatore, L. 2009, MNRAS, 400, 2000

Dijkstra, M., & Kramer, R. 2012, MNRAS, 424, 1672

Dijkstra, M., Mesinger, A., & Wyithe, J. S. B. 2011, MNRAS, 414, 2139

Foreman-Mackey, D., Hogg, D. W., Lang, D., & Goodman, J. 2013, PASP, 125, 306

Forero-Romero, J. E., Yepes, G., Gottlöber, S., Knollmann, S. R., Cuesta, A. J., & Prada, F. 2011, MNRAS, 415, 3666

Forero-Romero, J. E., Yepes, G., Gottlöber, S., & Prada, F. 2012, MNRAS, 419, 952

Garel, T., Blaizot, J., Guiderdoni, B., Schaerer, D., Verhamme, A., & Hayes, M. 2012, MNRAS, 422, 310

Gawiser, E., Francke, H., Lai, K., Schawinski, K., Gronwall, C., Ciardullo, R., Quadri, R., Orsi, A., Barrientos, L. F., Blanc, G. A., Fazio, G., & Feldmeier, J. J. 2007a, ApJ, 671, 278

Gawiser, E., Francke, H., Lai, K., Schawinski, K., Gronwall, C., Ciardullo, R., Quadri, R., Orsi, A., Barrientos, L. F., Blanc, G. A., Fazio, G., Feldmeier, J. J., Huang, J.-s., Infante, L., Lira, P., & Padilla, N. 2007b, ApJ, 671, 278
Guaita, L., Francke, H., Gawiser, E., Bauer, F. E., Hayes, M., Östlin, G., & Padilla, N. 2013, A&A, 551, A93
Hayashino, T., Matsuda, Y., Tamura, H., Yamauchi, R., Yamada, T., Ajiki, M., Fujita, S. S., Murayama, T., Nagao, T., Ohta, K., Okamura, S., Ouchi, M., Shimasaku, K., Shioya, Y., & Taniguchi, Y. 2004, AJ, 128, 2073
Jose, C., Srianand, R., & Subramanian, K. 2013, ArXiv e-prints
Klypin, A., Yepes, G., Gottlober, S., Prada, F., & Hess, S. 2014, ArXiv e-prints
Klypin, A. A., Trujillo-Gomez, S., & Primack, J. 2011, ApJ, 740, 102
Koehler, R. S., Schuecker, P., & Gebhardt, K. 2007, A&A, 462, 7
Landy, S. D., & Szalay, A. S. 1993, ApJ, 412, 64
Laursen, P., Duval, F., & Östlin, G. 2013, ApJ, 766, 124
Laursen, P., & Sommer-Larsen, J. 2007, ApJ, 657, L69
Neufeld, D. A. 1991, ApJ, 370, L85
Nilsson, K. K., Møller, P., Möller, O., Fynbo, J. P. U., Michałowski, M. J., Watson, D., Ledoux, C., Rosati, P., Pedersen, K., & Grove, L. F. 2007, A&A, 471, 71
Orsi, A., Lacey, C. G., & Baugh, C. M. 2012, MNRAS, 425, 87
Ouchi, M., Shimasaku, K., Akiyama, M., Simpson, C., Saito, T., Ueda, Y., Furusawa, H., Sekiguchi, K., Yamada, T., Kodama, T., Kashikawa, N., Okamura, S., Iye, M., Takata, T., Yoshida, M., & Yoshida, M. 2008, ApJS, 176, 301
Ouchi, M., Shimasaku, K., Furusawa, H., Saito, T., Yoshida, M., Akiyama, M., Ono, Y., Yamada, T., Ota, K., Kashikawa, N., Iye, M., Kodama, T., Okamura, S., Simpson, C., & Yoshida, M. 2010, ApJ, 723, 869
Peebles, P. J. E. 1980, The large-scale structure of the universe
Planck Collaboration, Ade, P. A. R., Aghanim, N., Armitage-Caplan, C., Arnaud, M., Ashdown, M., Atrio-Barandela, F., Aumont, J., Baccigalupi, C., Banday, A. J., & et al. 2014, A&A, 571, A16
Riebe, K., Partl, A. M., Enke, H., Forero-Romero, J., Gottlber, S., Klypin, A., Lemson, G., Prada, F., Primack, J. R., Steinmetz, M., & Turchaninov, V. 2013, Astronomische Nachrichten, 334, 691
Springel, V., White, S. D. M., Jenkins, A., Frenk, C. S., Yoshida, N., Gao, L., Navarro, J., Thacker, R., Croton, D., Helly, J., Peacock, J. A., Cole, S., Thomas, P., Couchman, H., Evrard, A., Colberg, J., & Pearce, F. 2005, Nature, 435, 629
Verhamme, A., Schaerer, D., & Maselli, A. 2006, A&A, 460, 397
Yajima, H., Choi, J.-H., & Nagamine, K. 2012, MNRAS, 427, 2889